Characterization of fracture aperture by inverse analysis

ANDREW R. PIGGOTT

National Water Research Institute, 867 Lakeshore Road, Burlington, Ont., Canada L7R 4A6

AND

DEREK ELSWORTH

Department of Mineral Engineering, Pennsylvania State University, 104 Mineral Sciences Building, University Park, PA 16802, U.S.A.

Received June 6, 1992

Accepted April 6, 1993

Formulation and application of a procedure for characterizing the spatial distribution of aperture within a single fracture in rock are discussed. A simultaneous-inversion approach is used to construct the aperture distribution that best replicates the variability apparent in measured hydraulic and electrical data. In this approach, aperture distributions are generated from a specified model, flow is simulated for each of multiple test types and configurations, the error of approximating the measured data with the simulated results is evaluated, and an optimization algorithm is used to minimize the error with respect to parameters regulating the aperture distribution. The procedure is applied to data obtained from laboratory tests conducted on a natural fracture in granite. Three aperture distributions with similar macroscopic characteristics are inferred from the data. Corroboration of these distributions is obtained from the simulation of tracer transport within the fracture and comparison of the simulated results with measured data.

Key words: characterization, fractured rock, groundwater flow, contaminant transport, inverse analysis.

La formulation et l'application d'une procédure pour caractériser la distribution spatiale d'ouverture à l'intérieur d'une fracture simple dans la roche sont discutées. Une approche d'inversion simultanée est utilisée pour construire la distribution d'ouverture qui reproduit le mieux la variabilité mise en évidence par les données hydrauliques et électriques. Dans cette approche, les distributions d'ouverture sont générées à partir d'un modèle spécifié, l'écoulement est simulé pour chacun des multiples types d'essais et configurations, l'erreur d'approximation des données mesurées au moyen des résultats simulés est évaluée, et un algorithme d'optimisation est utilisé pour minimiser l'erreur par rapport aux paramètres contrôlant la distribution d'ouverture. La procédure est appliquée aux données obtenues par des essais de laboratoire réalisés sur une fracture naturelle dans le granit. Trois distributions d'ouverture avec des caractéristiques macroscopiques similaires sont déduites des données. Une corroboration de ces distributions est obtenue par la simulation d'un transport de traceur à l'intérieur de la fracture et par une comparaison des résultats simulés avec les données mesurées.

Mots clés : caractérisation, roc fracturé, écoulement souterrain, transport de contaminant, analyse inverse.

[Traduit par la rédaction]

Can. Geotech. J. 30, 637–646 (1993)

Introduction

The extent to which a rock mass is transected by fractures, and other geologic discontinuities, is known to strongly regulate groundwater flow and contaminant transport. Fractures often greatly enhance the hydraulic conductivity of formations of low matrix hydraulic conductivity and may channelize flow in these formations, thus accelerating contaminant transport. The assessment of groundwater flow and contaminant transport in sparsely fractured rock masses is particularly important with regard to the siting and design of hazardous waste isolation facilities. Considerable progress in understanding the relation between fracturing and the hydrogeological behaviour of rock masses has recently been achieved; a comprehensive review of this progress is presented by Wang (1991).

To describe flow and transport through fractured rock masses, it is first necessary to characterize fracturing at two scales, namely, the larger scale of fracture systems and the smaller scale of single fractures. Characterization of fracturing at the scale of fracture systems involves defining the location, orientation, extent, and equivalent hydraulic and transport properties of the constituent fractures. This task has only recently been addressed in the literature (Billaux et al. 1989; Long et al. 1991; Martel and Peterson 1991).

Characterization of fracturing at the scale of single fractures involves defining the spatial distribution of aperture within the fractures. Brown et al. (1986) inferred the distribution of aperture within fracture specimens from the mismatch of profiles of the upper and lower surfaces of the fractures. Gale (1987) measured aperture distributions by injecting resin into compressed specimens and profiling the casts exposed in sections through the specimens. Pyrak-Nolte et al. (1987) studied the distribution of fracture surface-to-surface contact by injecting a low melting point alloy into compressed specimens and interpreting the casts using image-analysis techniques. Hakami (1988) estimated apertures at points within transparent fracture replicas by measuring the areas occupied by known volumes of water compressed between the fracture surfaces and then calculating aperture as the ratio of volume to wetted area. Wang et al. (1988) developed expressions for the spectral and geostatistical characteristics of aperture distributions from similar descriptions of fracture surfaces. Gentier and Billaux (1989) injected translucent resin into specimens and determined the distribution of aperture from the attenuation of light transmitted through the cast.

The preceding studies, with the exception of Wang et al. (1988), characterized the distribution of aperture through

Printed in Canada / Imprimé au Canada

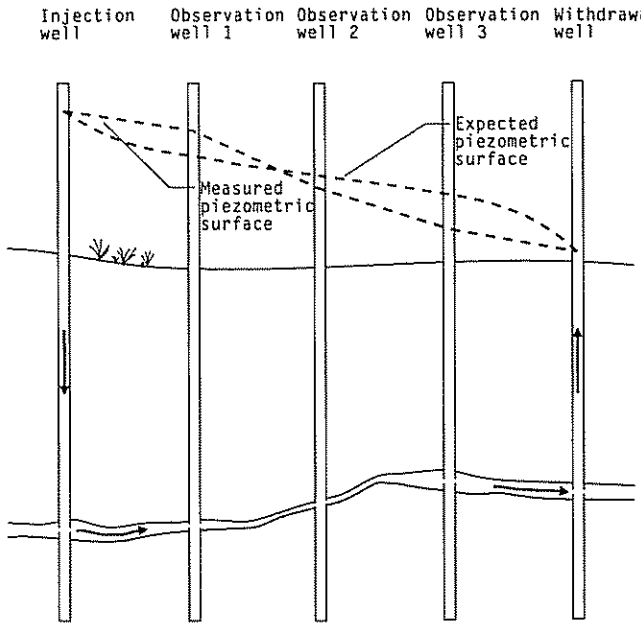

FIG. 1. Illustration of an in situ characterization test performed on an isolated fracture. The discrepancy between the expected and measured piezometric surfaces is the result of the diminished aperture in the vicinity of observation well 2.

direct measurement of fracture void geometry. This paper describes the characterization of aperture using an indirect procedure based on inverse analysis. In this approach, the macroscopic variability of flow within a fracture is used to construct a deterministic estimate of the macroscopic details of the distribution of aperture.

In forward application of numerical simulation, a model and distribution of properties is assumed, boundary conditions are stipulated, loading specified, and the response of the system to this loading predicted. If the simulated response of the system differs from the measured response, the discrepancy is often attributed to uncertainty in the estimation of the properties. In some cases, the properties are then adjusted until an improved match is obtained. Inverse analysis formalizes this procedure by defining an error function as a measure of the discrepancy between the simulated and measured responses and minimizing the error function with respect to each of the properties. The properties associated with the minimum error are then assumed to be those of the system.

Figure 1 illustrates a hydraulic characterization test performed on an isolated fracture in a low matrix hydraulic conductivity formation. Fluid is injected at one well and withdrawn at a second well, and the elevation of the piezometric surface is recorded in the injection and withdrawal wells and in three observation wells. This is referred to as a characterization test because more data are collected than is necessary to define the equivalent properties of the fracture if the fracture is of known geometry and assumed uniform aperture. Only the head loss between the injection and withdrawal wells and the injection rate are required to compute the equivalent aperture of the fracture, thus the observation wells provide additional information that may be used to characterize the fracture. A region of diminished aperture is apparent in the vicinity of observation well 2. This anomaly results in a deviation in the measured hydraulic heads from expected values corresponding to a uniform distribution of aperture. Intuitively, it is possible to infer characteristics of the aperture anomaly from the deviation in the measured data. Inverse analysis provides a formal basis for this inference.

The aperture distribution estimated in this manner is inherently associated with the scale of the observations, this scale being indexed by the spacing of the wells. Aperture variations at smaller scales produce deviations in the piezometric surface at similar small scales, and these deviations may not be apparent in the measured data. Because the measured data are not sensitive to small-scale aperture variations, these variations cannot be characterized from the measured data. Aperture variations at scales larger than that of the observations cannot be characterized because these variations also have limited expression in the measured data. The term macroscopic is used to denote variability at the scale of the observations.

Only one of many test configurations is illustrated in Fig. 1. For example, fluid could also be injected at observation well 1 and withdrawn at observation well 3. Each test configuration generates data corresponding to a different configuration of boundary conditions. In addition, tracer transport or electrical current transmission could be measured between the wells. All of the test configurations and types (hydraulic flow, tracer transport, and electrical current transmission) respond to the same distribution of aperture. However, the various configurations and transport processes are not redundant in that they are sensitive to different aspects of the aperture distribution. For example, radially divergent flow is most sensitive to apertures in the vicinity of the injection well. Hydraulic and electrical flow exhibit cubic and linear sensitivities to aperture variations, respectively. It is possible to propose an analytical approach that simultaneously considers all available data and relates these data to a single estimate of the aperture distribution. The merits of this approach are illustrated by Piggott et al. (1991).

The procedure for the characterization of aperture discussed in this paper is based on the simultaneous inversion of data describing fluid flow and electrical current transmission. Both processes are reliably represented in variable-aperture fractures using conventional methods of numerical simulation. Conceptually, the inclusion of tracer test results is straightforward. Tracer transport in variable-aperture fractures is not described in a robust manner using existing numerical simulation procedures, and therefore simultaneous inversion cannot yet be extended to include the results of tracer tests.

Formulation of the inversion algorithm

If fluid flow and electrical current transmission within a variable-aperture fracture are represented by the symbolic relation

$$[1] \quad \boldsymbol{D}_m = F(\boldsymbol{b})$$

where $F(\boldsymbol{b})$ relates the spatial distribution of aperture, $\boldsymbol{b}$, to measured data describing flow, $\boldsymbol{D}_m$, then inversion of the measured data to yield the aperture distribution is symbolically represented by

$$[2] \quad \boldsymbol{b} = F^{-1}(\boldsymbol{D}_m)$$

Inversion of the data is typically implemented in an algorithmic form. The actions of the algorithm are

(*i*) manipulation of the measured data
(*ii*) generation of candidate aperture distributions
(*iii*) approximation of the measured data using the current estimate of the aperture distribution
(*iv*) evaluation of the quality of the approximation, and
(*v*) optimization of the approximation with respect to the aperture distribution.

Detailed discussions of the first four of these actions are presented is this paper. Because numerous solutions to the optimization problem are available, only the selection of an appropriate solution methodology and the specification of the problem are discussed.

Measured data record

Measured hydraulic heads or electrical potentials for multiple measurement points and a particular test configuration may be expressed in vector notation. The syntax of this vector is

$$[3] \quad \boldsymbol{d}_{m,i}^{T} = [d_{m,i,1}\ d_{m,i,2}\ \cdots\ d_{m,i,N_m}]$$

where the entries of the vector are the data for each measurement point, N_m is the number of measurement points, and superscript T indicates vector transpose. The number of measurement points is constant for all tests conducted on a given specimen. An arbitrary value is used in place of a missing quantity to maintain the form of the vector if data for a particular measurement point and test are unavailable. The N_s sets of measured data, resulting from various test types and configurations may be assembled into a data record with the matrix syntax

$$[4] \quad \boldsymbol{D}_m = [\boldsymbol{d}_{m,1}\ \boldsymbol{d}_{m,2}\ \cdots\ \boldsymbol{d}_{m,N_s}]$$

Aperture distributions

To generate an estimate of the distribution of aperture within a fracture, it is first necessary to specify a model of the variation of aperture within the fracture. This model describes how aperture varies but does not describe actual aperture magnitudes. The aperture-distribution model is most conveniently expressed using a vector of N_p physical parameters

$$[5] \quad \boldsymbol{p}^{T} = [p_1\ p_2\ \cdots\ p_{N_p}]$$

and a vector of interpolating functions

$$[6] \quad (x,y)^{T} = [\boldsymbol{\Phi}_1(x,y)\ \Phi_2(x,y)\ \cdots\ \Phi_{N_p}(x,y)]$$

The spatial variation of aperture is then given by

$$[7] \quad b(x,y) = \boldsymbol{\Phi}\,(x,y)^{T}\,\boldsymbol{p}$$

It is necessary to define this continuous distribution of aperture at a number of predetermined positions (e.g., the locations of computational nodes) to simulate flow through a fracture. Interpolation of the aperture distribution at N_n nodal point locations may be performed using

$$[8] \quad \boldsymbol{b} = \boldsymbol{T}_b\,\boldsymbol{p}$$

where $\boldsymbol{b}$ is a vector of nodal apertures with

$$[9] \quad \boldsymbol{b}^{T} = [b_1\ b_2\ \cdots\ b_{N_n}]$$

The interpolation matrix has the form

$$[10] \quad \boldsymbol{T}_b = \begin{bmatrix} \Phi_1(x_{n,1},y_{n,1}) & \Phi_2(x_{n,1},y_{n,1}) & \cdots & \Phi_{N_p}(x_{n,1},y_{n,1}) \\ \Phi_1(x_{n,2},y_{n,2}) & \Phi_2(x_{n,2},y_{n,2}) & \cdots & \Phi_{N_p}(x_{n,2},y_{n,2}) \\ \vdots & \vdots & & \vdots \\ \Phi_1(x_{n,N_n},y_{n,N_n}) & \Phi_2(x_{n,N_n},y_{n,N_n}) & \cdots & \Phi_{N_p}(x_{n,N_n},y_{n,N_n}) \end{bmatrix}$$

in which $(x_{n,i},y_{n,i})$ denotes the nodal point locations.

Calculated data record

Flow through a variable-aperture fracture may be simulated using any of various numerical approaches. The finite element method was implemented in this study on the basis of both the accuracy and flexibility offered by the method; however, the procedure is independent of the method of flow simulation, and any suitable approach may be employed. Using the finite element method, flow is mathematically represented by

$$[11] \quad \boldsymbol{K}_{g,i}\,\boldsymbol{d}_{c,i} = \boldsymbol{q}_{c,i}$$

In [11], $\boldsymbol{K}_{g,i}$ is the global hydraulic or electrical conductance matrix evaluated for the current estimate of the aperture distribution, $\boldsymbol{d}_{c,i}$ is the vector of nodal hydraulic heads or electrical potentials for a particular boundary-condition configuration, and $\boldsymbol{q}_{c,i}$ is the corresponding vector of nodal fluid or electrical discharge.

The global conductance matrix is assembled following standard finite element procedures using

$$[12] \quad \boldsymbol{K}_{g,i} = \sum_{j=1}^{N_n} t_j \boldsymbol{K}_{n,j}$$

with t_j defined as the hydraulic or electrical transmissivity of the fracture at node j and $\boldsymbol{K}_{n,j}$ as the global conductance matrix formulated for a transmissivity of unity at node j and zero at all other nodes. In this implementation, the nodal conductance matrices are formulated at the element level using an isoparametric finite element procedure (Huyakorn and Pinder 1983) where the distribution of transmissivity within each element is interpolated from nodal values using the shape functions applied in element formulation. The variation of aperture within each element is therefore explicitly factored into the elemental conductance matrices.

For fluid flow, the nodal transmissivities derived from the parallel plate analogy are

$$[13] \quad \boldsymbol{t}^{T} = \frac{g}{12\,\nu}[b_1^3\ b_2^3 \cdots b_{N_n}^3]$$

where g is gravitational acceleration, and ν is the kinematic viscosity of the fluid. For electrical current flow, the nodal transmissivities are

$$[14] \quad \boldsymbol{t}^{T} = k_e[b_1\ b_2\ \cdots\ b_{N_n}]$$

where k_e is the electrical conductivity of the fluid saturating the fracture.

The calculated data record is assembled from the distributions of hydraulic head and electrical potential derived

by the solution of [11]. The syntax of the calculated data record is

$$[15] \quad \boldsymbol{D}_c = [d_{c,1}\ d_{c,2}\ \ldots\ d_{c,N_c}]$$

which is similar to that of the measured data record, that is, the columns in both records contain data corresponding to a particular test type and configuration. The quantities are defined at the measurement and nodal-point locations in the measured and calculated data records, respectively. In general, these locations do not coincide, and the final step in processing the calculated data record is interpolation of the calculated quantities at the measurement-point locations. This is represented by

$$[16] \quad \boldsymbol{D}_c \leftarrow \boldsymbol{T}_D\, \boldsymbol{D}_c$$

Through judicious discretization, it is generally possible to specify nodal locations that correspond to the locations of the measurement points. In this case, the entries of the interpolating matrix, T_D, are either unity or zero, arranged to return the nodal quantities corresponding to each measurement point.

Calculation of the error function

The error function describes the discrepancy between the measured data record and the calculated data record for the current estimate of the aperture distribution. An appropriate definition of the error function is

$$[17] \quad E(\boldsymbol{p}) = \sum_{i=1}^{N_m} \sum_{j=1}^{N_s} W_{i,j} \left| D_{c_{i,j}} - D_{m_{i,j}} \right|^2$$

where $W_{i,j}$ are weighting factors that regulate the contribution of the error increment for each measurement point and data set (the data for a particular test type and configuration). Several influences are reflected in these weighting factors. First, the weighting factors for each measurement point are proportional to the area of the specimen that is tributary to that point. This ensures that the error function is an expression of the average error over the area of the fracture. Second, the weighting factors for each data set are inversely proportional to a characteristic magnitude of the data. This ensures that the error increments for electrical data, which might be measured in volts, are not overwhelmed by the increments for hydraulic data, which might be measured in hundreds of millimetres. Failure to compensate for differing characteristic magnitudes causes the inversion algorithm to return an aperture distribution that is biased towards data sets with large characteristic magnitudes. Third, the weighting factors express a qualitative measure of confidence in the data and of the significance of the data to the analysis. Finally, if a measured or calculated quantity is unknown and assigned an arbitrary value, the corresponding weighting factor is assigned a value of zero.

Minimization of the error function

The best estimate of the aperture distribution is obtained by minimizing the error function with respect to the parameters regulating the distribution. This translates to an optimization problem in which the minimum of the error function corresponds to the optimality condition.

At this point, it is useful to apply the concept of parameter space, defined as the N_p-dimensional space associated with the physical parameters in the aperture distribution model. A single value of the error function exists for each point in parameter space, and each point defines a unique combination of the physical parameters and therefore a unique aperture distribution. The function of an optimization algorithm is to locate the point in parameter space corresponding to the minimum value of the error function.

Optimization algorithms

Selection of an optimization algorithm for a particular problem must take a number of factors into consideration. A brief review of these issues is presented here; more comprehensive discussions are presented by Gill et al. (1981) and Press et al. (1986).

Optimization problems can be divided into two categories. In continuous optimization problems, the parameters assume any value within a predetermined range of values. In discrete optimization problems, the parameters assume only specified values. The optimization problem defined here is continuous.

Certain solution procedures for continuous optimization problems require knowledge of the first and second derivatives of the error function (the gradient vector and Hessian matrix). If expressions for these quantities are available, then methods that utilize this information are frequently most effective. While the absence of expressions for the gradient vector and Hessian matrix does not preclude the use of these methods, the computational burden of estimating these quantities using numerical approaches is often not justified. Neither the gradient vector nor Hessian matrix are known in the present optimization problem.

A final factor to be considered in selecting an optimization algorithm is the potential for discontinuities or intense nonlinearity in the error function. In these cases, direct-search optimization algorithms are most appropriate. The error function defined previously displays marked nonlinearity.

The AMOEBA optimization algorithm of Press et al. (1986) was selected for use in this study. This algorithm is applicable to continuous optimization problems and does not require calculation of the gradient vector or Hessian matrix. Additionally, the algorithm accommodates the nonlinearity of the error function.

The AMOEBA algorithm is an implementation of the polytope direct-search procedure. A polytope is a N_p-dimensional geometric form defined by $N_p + 1$ vertices (e.g., a tetrahedron in three-dimensional parameter space). The error function is evaluated at each of the vertices, and a motion of the polytope is selected based on a comparison of these error-function values. Through a series of motions, the polytope moves towards a minimum of the error function. Successful applications of polytope optimization algorithms to geomechanics problems are noted in the literature (Gioda and Maier 1980; Cividini et al. 1981).

Two conditions in inverse analysis warrant special consideration. The first occurs when multiple points in parameter space have the same minimum value of the error function. Since these points correspond to equally accurate approximations of the measured data, there is no unique best estimate of the physical parameters. The second condition occurs when the parameter space contains local minima that optimization algorithms are often unable to distinguish from the global minimum. A test of the uniqueness of a solution is obtained by restarting the optimization algorithm with a different initial estimate of the parameters (Press et al. 1986). If the algorithm returns to the same point in parameter space, a unique solution is likely. If the algorithm locates a different point with a similar error-

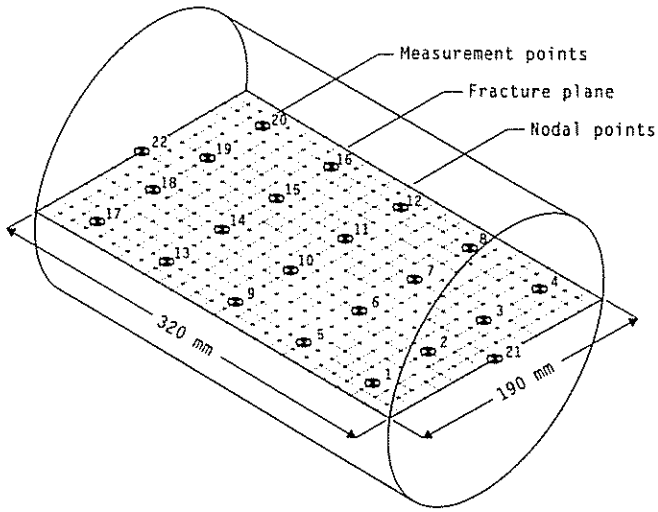

FIG. 2. Illustration of the fracture specimen showing the arrangement of measurement points and computational nodal points.

function magnitude, a nonunique solution is probable. Finally, if the algorithm locates a different point with a significantly different error-function magnitude, then one or both of the solutions may be local minima.

Parameter constraints

Minimization of the error function is often performed subject to constraints that restrict the values of the physical parameters. One form of constraint is the definition of permissible and impermissible regions of parameter space. For example, fracture aperture may be constrained within a range of values such that

$$[18] \quad b_{min} \le b(x,y) \le b_{max}$$

where b_{min} and b_{max} are specified minimum and maximum permissible apertures. This form of constraint may be implemented by examining the nodal apertures corresponding to the current estimate of the physical parameters and assigning an arbitrarily large value to the error function if the constraint is violated at any of the nodes. This forces the optimization algorithm to recoil from that region of parameter space.

A second form of constraint arises when the values of the physical parameters are explicitly related. For example, under laboratory conditions it is possible to measure the total volume of a fracture and determine volumetric mean aperture as the ratio of fracture volume to area. It is appropriate to require that the averages of the estimated aperture distributions are constant and equal to the measured volumetric mean aperture. In this case, the parameters must satisfy

$$[19] \quad p_1 \int_{A_f} \Phi_1(x,y)\,dA + p_2 \int_{A_f} \Phi_2(x,y)\,dA + \cdots + p_{N_p} \int_{A_f} \Phi_{N_p}(x,y)\,dA = A_f b_v$$

with A_f and b_v defined as the area and volumetric mean aperture of the fracture, respectively. Relations analogous to [19] may be written if aperture is known at points within the fracture as the result of direct measurements.

Each constraint in the form of [19] reduces the number of degrees of freedom in the optimization problem by one.

TABLE 1. Equivalent hydraulic apertures determined from point-source tests (Piggott 1990)

Injection point	Aperture (mm)
9	0.15
10	0.14
11	0.18
12	0.17
17	0.12
18	0.12
19	0.12
20	0.12

For example, if four physical parameters are defined, if volumetric mean aperture is known, and if aperture is known at one point in the fracture, then the reduced dimension of the optimization problem is two, i.e., $N_r = 4 - 2 = 2$. The solution to this reduced-dimension problem is obtained by minimizing the error function with respect to a N_r-dimensional vector of optimization parameters, $\boldsymbol{r}$. The physical parameters and optimization parameters are related via

$$[20] \quad \boldsymbol{p} = \boldsymbol{T}_p \boldsymbol{r} + \boldsymbol{p}_o$$

Here, $\boldsymbol{p}_o$ is any estimate of the physical parameters that satisfies the constraints, and the syntax of $\boldsymbol{T}_p$ is

$$[21] \quad \boldsymbol{T}_p = [\nu_1\ \nu_2\ \cdots\ \nu_{N_r}]$$

where ν_i are N_p-dimensional basis vectors that span the portion of physical parameter space which is permissible subject to constraints with the form of [19].

Constraints such as [18] prohibit the optimization algorithm from entering unreasonable regions of parameter space (e.g., regions associated with nodal apertures that are substantially less than or greater than realistic values). This avoids the formulation of poorly conditioned simulation problems and decreases the computational burden of an analysis by decreasing the number of parameter-value combinations that must be examined. Constraints such as [19] reduce the number of degrees of freedom in the optimization problem and therefore also decrease the computational burden of an analysis.

Application to laboratory data

The results of laboratory tests reported by Piggott (1990) are suitable for analysis using the procedure described in this paper. These results were selected for this initial application of the aperture-characterization procedure on the basis that the geometry of the specimen and boundary conditions are known, thereby eliminating uncertainty in these quantities from the complications of the analysis.

The tests were performed on a natural fracture specimen in granite obtained from the Underground Research Laboratory of Atomic Energy of Canada Limited. Details of the geology of the site and the extraction of the specimen are presented by Lang (1986). The fracture is oriented along the axis of a 190 mm diameter by 320 mm long core. Twenty 5 mm diameter holes were drilled through the core to form the array of measurement points shown in Fig. 2. Each measurement point was instrumented with flexible tubing and two-conductor copper wire. The tubing was used to measure hydraulic heads and to inject fluid into the frac-

TABLE 2. Summary of the measured data

Measurement point	Injection point									
	22[a]	22[b]	9[a]	10[a]	11[a]	12[a]	17[a]	18[a]	19[a]	20[a]
1	0.079	0.118	0.132	0.110	0.216	0.188	0.039	0.039	0.041	0.041
2	0.091	0.123	0.147	0.140	0.284	0.256	0.051	0.050	0.052	0.050
3	0.094	0.123	0.139	0.144	0.351	0.363	0.055	0.057	0.058	0.057
4	0.100	0.134	0.128	0.136	0.358	0.413	0.055	0.057	0.058	0.057
5	0.181	0.281	0.335	0.271	0.455	0.400	0.095	0.097	0.098	0.098
6	0.170	0.272	0.271	0.254	0.537	0.469	0.091	0.091	0.094	0.093
7	0.180	0.275	0.256	0.258	0.687	0.631	0.098	0.100	0.103	0.102
8	0.157	0.237	0.214	0.225	0.619	0.750	0.092	0.094	0.097	0.096
9	0.449	0.469	na[c]	0.754	0.634	0.563	0.317	0.320	0.319	0.320
10	0.459	0.457	0.838	na[c]	0.858	0.663	0.354	0.361	0.361	0.359
11	0.319	0.433	0.338	0.386	na[c]	0.869	0.159	0.162	0.166	0.166
12	0.299	0.420	0.308	0.326	0.925	na[c]	0.165	0.171	0.173	0.177
13	0.819	0.679	1.083	1.038	0.963	0.931	0.874	0.879	0.870	0.865
14	0.831	0.680	1.000	1.034	1.022	0.994	0.905	0.926	0.923	0.909
15	0.804	0.667	0.925	0.953	1.060	1.069	0.869	0.887	0.908	0.898
16	0.776	0.660	0.872	0.890	1.030	1.200	0.830	0.840	0.867	0.891
17	0.979	0.909	1.000	1.004	1.000	1.000	na[c]	1.000	0.992	0.993
18	0.953	0.870	1.004	1.000	1.007	1.000	0.988	na[c]	0.994	0.987
19	0.943	0.782	0.992	0.996	1.007	1.013	0.973	0.987	na[c]	1.007
20	0.946	0.863	0.981	0.983	1.007	1.013	0.973	0.980	1.008	na[c]

[a]Hydraulic data.
[b]Electrical data.
[c]Hydraulic heads at the injection point are not available for the point-source tests. Weighting factors of zero are assigned to these observations.

ture, the wire to measure electrical potentials and saline tracer breakthrough. The void volume introduced by the holes was minimized by filling the holes with sealant to the fracture surface. The remaining excess volume is of little consequence because the tests were conducted under conditions of steady-state flow. Tracer transport is most influenced by the excess volume, with the impact limited by minimizing the volume. Following instrumentation, the specimen was clamped circumferentially and the intersections of the fracture with the sides of the core were sealed. Platens were installed along the intersections of the fracture with the ends of the core. Channels within the platens distribute fluid and electrical current along these boundaries. Additional measurement points were then established at the centres of the platens.

Tests were conducted under nominally mated and sheared conditions. Only the results of the tests conducted under mated conditions are addressed here. Under sheared conditions, the average aperture of the fracture was large relative to the magnitude of spatial variations in aperture, and the aperture distribution did not generate significant variability in either hydraulic head or electrical potential. Characterization of the aperture distribution under sheared conditions would simply reflect the uniformity of the measured data.

The tests performed on the specimen included hydraulic tests in which fluid was injected at the bottom of the specimen (measurement point 22 in Fig. 2) and withdrawn at the top of specimen (measurement point 21). Electrical and tracer tests with the same configuration were also performed. Additionally, point-source hydraulic and tracer tests were conducted. Here, fluid was sequentially injected at measurement points 9–12 and 17–20 and withdrawn at the top of the specimen. The data collected from the tests include observations of hydraulic head, electrical potential, and tracer breakthrough at each measurement point where the observations correspond to the varying configuration of injection and withdrawal. A complete description of the experimental program and procedures is presented in Piggott (1990). Only hydraulic and electrical data are considered in inverse analysis. Tracer test results are used to assess the aperture distributions estimated from the hydraulic and electrical data.

The data collected during the point-source hydraulic tests are interpreted in Piggott (1990) as equivalent apertures, which are a measure of the average aperture encountered by fluid flowing from the injection point to outlet. Table 1 lists these equivalent apertures. Because of the divergent nature of the flow field in the vicinity of the injection points, the equivalent apertures are strongly weighted towards aperture magnitudes adjacent to the injection points. Two trends are apparent in the equivalent apertures. First, the apertures determined from injection at points 17–20 are less than those for points 9–12. Second, the apertures determined from injection at points 9 and 10 are less than those for points 11 and 12. These trends indicate a flow constriction between points 9–12 and 17–20 and suggest that this constriction persists between points 9 and 10 and the outlet. This observation supports the notion that the distribution of aperture within the fracture can be characterized from the measured data.

The data collected from tests conducted under mated conditions are summarized, in dimensionless form, in Table 2. In this form, each data set is translated and scaled using the data for points 21 and 22 such that the dimensionless values for points 21 and 22 are zero and unity, respectively. By rendering the data dimensionless in this manner, all of the data sets have roughly equivalent characteristic magnitudes.

TABLE 3. Tributary areas of the measurement points

Measurement point	Tributary area (mm^2)
1	2981.25
2	3312.50
3	3312.50
4	2981.25
5	2812.50
6	3125.00
7	3125.00
8	2812.50
9	2812.50
10	3125.00
11	3125.00
12	2812.50
13	2812.50
14	3125.00
15	3125.00
16	2812.50
17	2981.25
18	3312.50
19	3312.50
20	2981.25
Total	190 × 320 = 60 800

The calculated data are similarly translated and scaled prior to evaluating the error function.

The weighting factors for each of the observations were derived using

$$[22] \quad W_{i,j} = \frac{A_i}{A_f} w_j$$

where A_i is the tributary area of each measurement point, A_f is the total area of the fracture, and w_j is the weight assigned to each data set. Table 3 lists the tributary areas of the measurement points. Unit weights (w_j = 1) were specified for the data sets corresponding to injection at point 22. The point-source data, collectively, were also assigned a unit weight; thus, each set of point-source data was assigned a weight equal to one-eighth the weight for the data sets corresponding to injection at point 22 (w_j = 0.125).

Flow through the specimen was simulated using the array of 459 nodes and 416 four-noded elements shown in Fig. 2.

Analyses were conducted using the three aperture-distribution models illustrated in Fig. 3. Models 1 and 2 are based on a piecewise constant distribution of aperture where the aperture in each element is equal to the aperture defined at the central interpolating point. The geometry of model 1 was derived from the geometry of the array of measurement points. The geometry of model 2 was specified to yield a sparser parameterization (i.e., fewer parameters). The aperture distribution in model 3 is described by Lagrangian interpolating functions defined by the array of interpolating points. This model permits a quadratic variation of aperture across the width of the specimen and a cubic variation along the length of the specimen.

Minimum and maximum permissible apertures were arbitrarily specified as 0.0027 and 2.7 mm, and the measured volumetric mean aperture of 0.27 mm was specified as a constraint. This resulted in optimization problems with 17 optimization parameters for aperture-distribution model 1, 7 parameters for model 2, and 11 parameters for model 3.

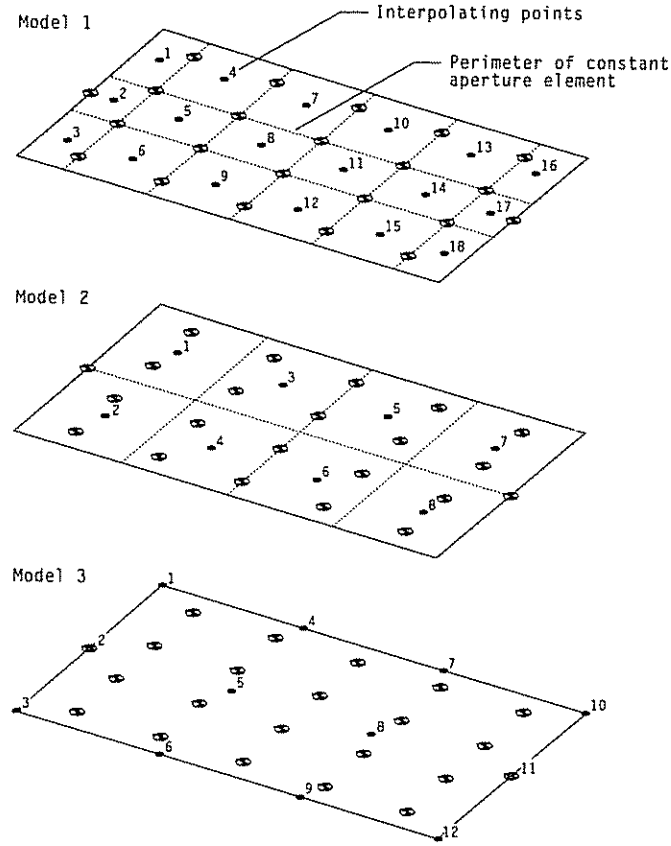

FIG. 3. Geometry of the aperture-distribution models. The aperture distributions in models 1 and 2 are piecewise constant, with the aperture in each element represented at the central interpolating point. The aperture distribution in model 3 is derived from Lagrangian interpolating functions defined by the array of interpolating points.

In all three analyses, optimization parameters corresponding to a uniform aperture distribution were specified as an initial estimate. This distribution yields an error-function magnitude of 4.58×10^{-2}. The vertices of the initial polytope were generated from the initial parameter estimate as described by Press et al. (1986). In accordance with the recommendations of Gioda and Maier (1980), the AMOEBA algorithm was modified to terminate only when both the optimization parameters and error-function magnitudes at the vertices of the polytope differ by less than a prescribed quantity (10^{-6} times the initial difference in these quantities). The algorithm was restarted once with the vertices of the second initial polytope generated from the estimate of the optimization parameters determined from the first application of the algorithm. The minimum error function magnitudes derived in this manner are 5.97×10^{-3}, 8.27×10^{-3}, and 9.37×10^{-3} for aperture distribution models 1, 2, and 3, respectively. Table 4 lists the final estimates of the physical parameters (i.e., the apertures at the interpolating points) corresponding to these minima. The minimum error function magnitude for aperture-distribution model 2 is greater than that for model 1. This is an expected result, since a decrease in the number of optimization parameters typically results in a degraded best approximation of the measured data. The minimum error-function magnitude for model 3 is greater than that for model 2 despite the fact that a larger number of optimization parameters are associated with

TABLE 4. Estimated apertures at the interpolating points

Interpolating point	Aperture (mm)		
	Model 1	Model 2	Model 3
1	0.229	0.283	0.850
2	0.294	0.386	0.649
3	0.390	0.153	0.516
4	0.220	0.201	0.133
5	0.369	0.315	0.144
6	0.255	0.207	0.239
7	0.157	0.313	0.388
8	0.165	0.326	0.241
9	0.190		0.245
10	0.335		0.199
11	0.173		0.179
12	0.224		0.431
13	0.407		
14	0.367		
15	0.363		
16	0.276		
17	0.062		
18	0.318		

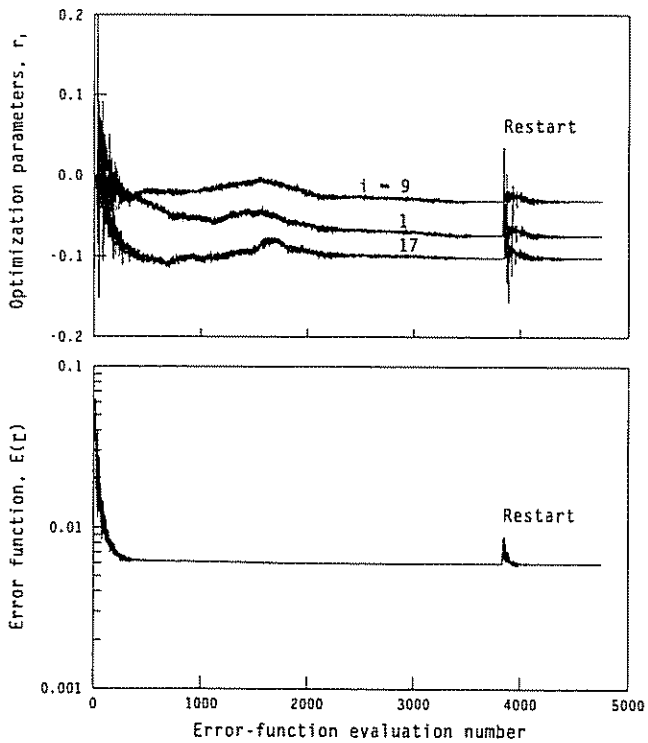

FIG. 4. Record of the values of optimization parameters 1, 9, and 17 (i = 1, 9, 17) and the error function for the analysis using aperture-distribution model 1.

model 3 than with model 2. A possible explanation for this outcome is that, unlike models 1 and 2, model 3 has a predetermined and continuous functional variation of aperture.

The values of the optimization parameters and error function were recorded each time the AMOEBA algorithm called the error-function calculation routine. Figure 4 shows the values of selected optimization parameters and the error function for the analysis using aperture-distribution model 1. The optimization parameters and error function converge to nearly constant values prior to the initial termination of the algorithm. Following restart, both the optimization parameters and error function return to effectively the same values as those obtained during the first application of the algorithm. This suggests that a unique best estimate of the aperture distribution exists for model 1. Similar results are noted for models 2 and 3.

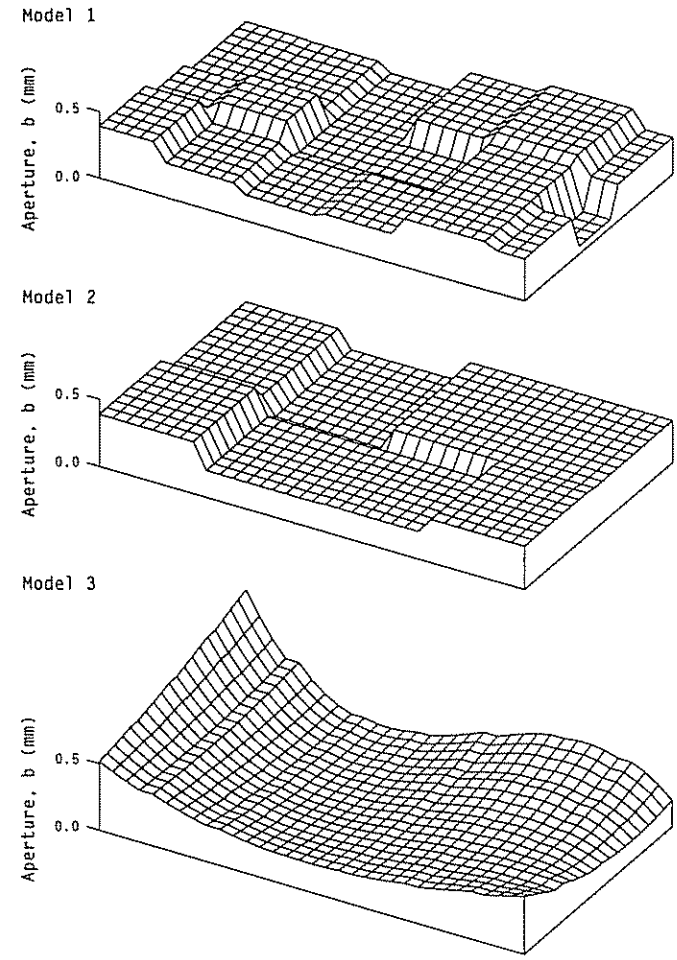

FIG. 5. Estimated aperture distributions.

Figure 5 shows the variations of aperture within the specimen corresponding to the aperture-distribution models shown in Fig. 3 and the estimated apertures listed in Table 4. Although details of the estimated aperture distributions differ as the result of the different underlying models, macroscopic similarities are apparent. All of the distributions display a region of diminished aperture approximately half-way along the length of the specimen, which widens and becomes less pronounced towards the right-hand side of the specimen.

As an independent evaluation of the estimated aperture distributions, the results of tracer tests conducted between measurement points 22 and 21 were simulated using the particle-tracking algorithm described by Piggott (1990). Studies indicate that this approach provides only a crude representation of tracer transport through variable-aperture fractures (Goode and Shapiro 1991), thus the simulated results are only a qualitative measure of tracer transport. Figure 6 compares the measured distribution of dimensionless tracer transit time to the simulated results for the three estimated aperture distributions. Dimensionless tracer transit times for each measurement point were calculated as the number of injected pore volumes of tracer solution corresponding to the median arrival time of the tracer. Mean

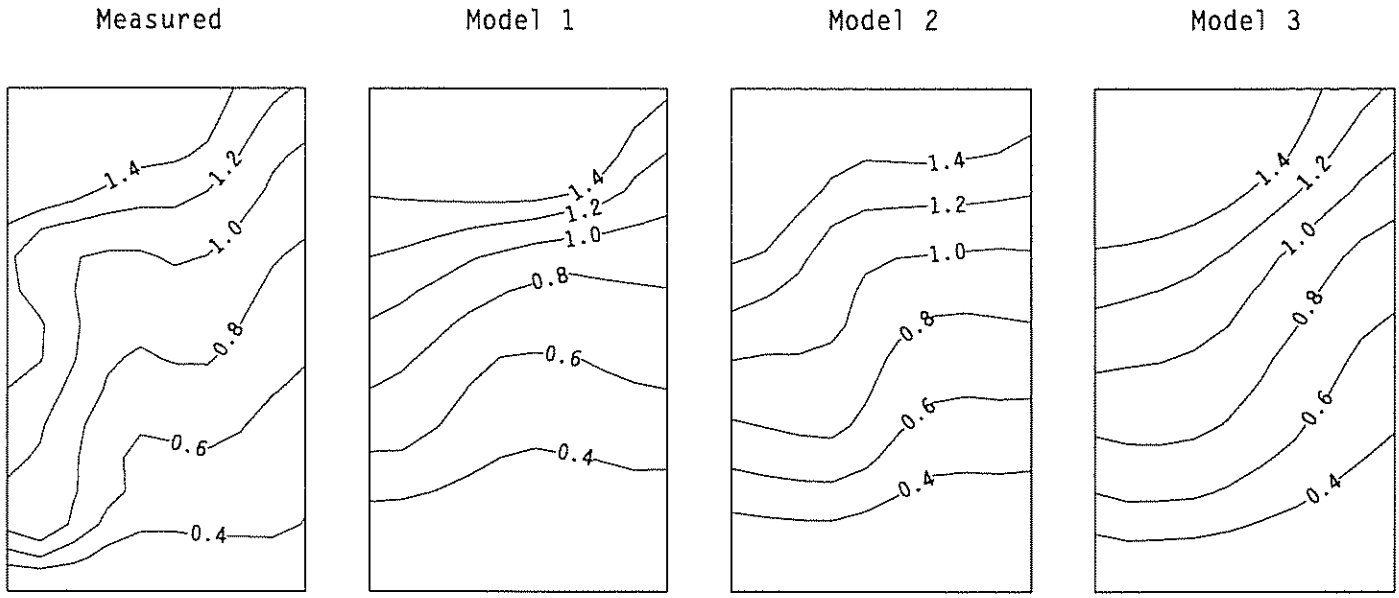

FIG. 6. Measured and simulated distributions of dimensionless tracer transit time. The tracer is injected along the bottom of the specimen and withdrawn along the top.

arrival times were substituted for median values in calculating the simulated results. The simulated results were then scaled to minimize the difference between the simulated and measured data. It is therefore appropriate to compare only the form of the measured and simulated distributions and not the magnitude of the results.

There is overall agreement between the forms of the measured and simulated results. However, the simulated results do not replicate the details of the measured distribution, and the correspondence should be regarded as qualitative. All of the distributions illustrate more rapid tracer transport along the right-hand side of the specimen than along the left-hand side. The estimated aperture distributions suggest that, overall, apertures along the right-hand side of the specimen are less than those along the left-hand side. This necessitates accelerated flow velocities because, if continuity is to be maintained, velocity must increase if aperture decreases. Additionally, the results consistently illustrate more rapid transport in the lower and central portions of the specimen than in the upper portion. The aperture distributions, particularly the distribution derived from model 1, indicate that the lower and central portions of the specimen are characterized by smaller apertures than the upper portion, again necessitating accelerated flow velocities.

Although there are discrepancies between the measured and simulated distributions of tracer transit time, the simulated results provide a better description of the variability of tracer transport than that derived from an equivalent aperture model (Piggott 1990). The equivalent aperture model assumes a uniform distribution of aperture and predicts a constant rate of tracer transport, with the resulting contours of tracer transit time appearing as uniformly spaced, linear features oriented perpendicular to the overall direction of tracer transport.

Discussion and conclusions

The aperture-characterization procedure is applicable to interpretation of hydraulic and electrical data describing flow through a single fracture in a lithology of low matrix conductivity. Studies to date have shown the procedure to be robust and efficient. Computational implementation of the procedure follows directly from the algorithm described herein. The code is compact and was developed and executed on a 25-MHz 486 personal computer using an extended-memory FORTRAN compiler. Computational times varied from 1 h for aperture-distribution for model 3 to 6 h for model 1.

The estimated aperture distributions display similar characteristics at the macroscopic scale, notably a region of diminished aperture. The equivalent apertures derived from the point-source tests support both the location and geometry of this region. Additionally, the agreement between the measured and simulated tracer transit time distributions supports the validity of the aperture distributions. Based on these results, it appears that the variability of flow within the fracture specimen is largely the product of the region of diminished aperture. It is likely that this anomaly is the result of a mismatch of the two halves of the specimen. Inspection of the topography of the fracture surface reveals a pronounced offset in the vicinity of the anomaly that could produce a region of diminished aperture if the specimen were subjected to an appropriate shear displacement.

Replication of the tracer test results is a significant outcome of this study. This demonstrates that, at least in this case, the contaminant transport behaviour of a fracture can be approximated from the analysis of hydraulic and electrical data. This conclusion has implications at in situ scales, where hydraulic tests are more conveniently performed than tracer tests, and at laboratory scales, where high-resolution electrical data could be obtained and used to derive detailed characterizations of aperture.

This application of the aperture-characterization procedure focuses on laboratory data. Application of the procedure in situ is possible because similar tests can be conducted and the analytical approach can be revised to accommodate the changed configuration of the flow regime. For an in situ application of the procedure, the boundary conditions applied to the numerical model must represent flow beyond the instrumented portion of the fracture.

Billaux, D., Chiles, J.P., Hestir, K., and Long, J. 1989. Three-dimensional statistical modelling of a fractured rock mass — an example from the Fanay–Augères Mine. International Journal of Rock Mechanics, Mining Sciences and Geomechanics Abstracts, **26**: 281–299.

Brown, S.R., Kranz, R.L., and Bonner, B.P. 1986. Correlation between the surfaces of natural rock joints. Geophysical Research Letters, **13**: 1430–1433.

Cividini, A., Jurina, L., and Gioda, G. 1981. Some aspects of characterization problems in geomechanics. International Journal of Rock Mechanics, Mining Sciences and Geomechanics Abstracts, **18**: 487–503.

Gale, J.E. 1987. Comparison of coupled fracture deformation and fluid flow models with direct measurements of fracture pore structure and stress-flow properties. *In* Proceedings of the 28th U.S. Symposium on Rock Mechanics, June 29–July 1, 1987, Tucson, Ariz. *Edited by* I.W. Farmer, J.J.K. Daemen, C.S. Desai, C.E. Glass, and S.P. Neuman. A.A. Balkema, Rotterdam. pp. 1213–1222.

Gentier, S., and Billaux, D. 1989. Caractérisation en laboratoire de l'espace fissural d'une fracture. *In* Rock at great depth. *Edited by* V. Maury and D. Fourmaintraux. A.A. Balkema, Rotterdam. pp. 425–431.

Gill, P.E., Murray, W., and Wright, M. 1981. Practical optimization. Academic Press, New York.

Gioda, G., and Maier, G. 1980. Direct search solution of an inverse problem in elastoplasticity: Identification of cohesion, friction angle and in situ stress by pressure tunnel tests. International Journal for Numerical Methods in Engineering, **15**: 1823–1848.

Goode, D.J., and Shapiro, A.M. 1991. Comment on "Flow and tracer transport in a single fracture: A stochastic model and its relation to some field observations" by L. Moreno et al. Water Resources Research, **27**: 129–131.

Hakami, E. 1988. Water flow in single rock joints. Licentiate thesis 1988:11 L, Luleå University of Technology, Luleå, Sweden.

Huyakorn, P.S., and Pinder, G.F. 1983. Computational methods in subsurface flow. Academic Press, Orlando, Fla.

Lang, P.A. 1986. Overview of the fracture testing program at the Underground Research Laboratory. Atomic Energy of Canada Limited Research Company, Chalk River, Ont. Technical Record TR-408.

Long, J.C.S., Karasaki, K., Davey, A., Peterson, J., Landsfeld, M., Kemeny, J., and Martel, S. 1991. An inverse approach to the construction of fracture hydrology models conditioned by geophysical data. International Journal of Rock Mechanics, Mining Sciences and Geomechanics Abstracts, **28**: 121–142.

Martel, S.J., and Peterson, J.E. 1991. Interdisciplinary characterization of fracture systems at the US/BK site, Grimsel Laboratory, Switzerland. International Journal of Rock Mechanics, Mining Sciences and Geomechanics Abstracts, **28**: 295–323.

Piggott, A.R. 1990. Analytical and experimental studies of rock fracture hydraulics. Ph.D. thesis, Pennsylvania State University, University Park, Penn.

Piggott, A.R., Xiang, J., and Elsworth, D. 1991. Inversion of hydraulic and electrical data for the determination of fracture aperture. *In* Rock mechanics as a multidisciplinary science. July 10–12, 1991, Norman, Okla. *Edited by* J.-C. Roegiers. A.A. Balkema, Rotterdam. pp. 1135–1144.

Press, W.H., Flannery, B.P., Teukolsky, S.A., and Vetterling, W.T. 1986. Numerical recipes, the art of scientific computing. Cambridge University Press, New York.

Pyrak-Nolte, L.J., Myer, L.R., Cook, N.G.W., and Witherspoon, P.A. 1987. Hydraulic and mechanical properties of natural fractures in low permeability rock. *In* Proceedings of the 6th International Congress on Rock Mechanics, Aug. 30–Sept. 3, 1987, Montréal, Que. *Edited by* G. Herget and S. Vongpaisal. A.A. Balkema, Rotterdam. Vol. 1. pp. 225–231.

Wang, J.S.Y. 1991. Flow and transport in fractured rock. U.S. National Report to the International Union of Geodesy and Geophysics 1987–1990, Contributions in Hydrology, Reviews of Geophysics Supplement, American Geophysical Union, Washington, D.C. pp. 254–262.

Wang, J.S.Y., Narasimhan, T.N., and Scholz, C.H. 1988. Aperture correlation of a fractal fracture. Journal of Geophysical Research, B, **93**: 2216–2224.